International Journal of Applied Engineering Research
ISSN 0973-4562 Volume 10, Number 7 (2015) pp. 16261-16282

http://www.ripublication.com

Grey Box System Identification And Optimal Control Of A Single Link Flexible Manipulator With Acld Treatment Using Stand – Off – Layer

Rajiv Kumar

Professor, Department of Mechanical Engg., Lovely Professional University
Jalandhar (Punjab) INDIA
**rkvashishat@yahoo.com*

Abstract:

Accurate trajectory regulation of flexible link manipulators is a challenging task. During hub angle regulation, the tip or the end-effector of the flexible manipulator undergoes excessive vibrations. Using active vibration control techniques on the piezoelectric materials attached on the flexible link the amplitude and duration of these vibrations can be reduced. Apart from these active control techniques, passive damping techniques are robust, effective and fail safe. The most important property of these techniques is that they don't require any actuation energy to obtain the necessary damping of the flexible link. Passive constrained layer damping (PCLD) is an old technique to suppress vibrations. It has also been observed that by applying the Stand-of-Layer between flexible structure and the viscoelastic layer, effective damping can be increased. In combination with active control techniques, these passive treatments can be made even more effective. In the present work, the effectiveness of these active/passive techniques has been investigated to reduce the end-effector vibrations during hub angle regulation.

1. Introduction and Problem Formulation

Robotic manipulators are widely used to help in dangerous, monotonous, and tedious jobs. The existing heavy rigid manipulators are shown to be inefficient in terms of power consumption or speed with respect to the operating payload. For these purposes it is very desirable to build flexible robotic manipulators. Due to the importance and usefulness of these topics, researchers worldwide are now-a-days engaged in the investigation of dynamics and control of flexible manipulator [1-5].

In order to achieve high precision in tip positioning, the use of tip position measurement is essential. In ref. [6], Canon and Schmitz initiated the experiment to control the tip positioning of flexible manipulator by using measurement from a tip positioning sensor as a feedback input. They designed a Linear Quadratic Gaussian

(LQG) controller and the obtained satisfactory step response with accurate tip positioning. To compensate the modeling errors, robust controllers based on H∞ optimization were used.

To enhance the flexible link's vibration damping property, additional sensors and actuators can be applied [7]. By using piezoceramic actuators (i.e. lead zirconate titnate or PZT patches) bonded to the flexible link, the link vibrations can be suppressed through a combination of hub motion control and control of PZT actuators. In the context of PZT patch control design, Sun et al [8] studied the active vibration control of flexible link damping problem using a combined scheme of hub PD (proportional derivative) feedback and linear velocity (so called 'L-type') feedback of PZT actuators. In ref. [9] Shaw et al showed that the L-type control of the distributed PZT patches was only conditionally stable and that to ensure stability, the PZT patches had to be placed in spots where the curvature of the link would not inflect across the domain of the patch. This work was extended to rotating cantilever beams in references [10-11]. Only recently, Gurses et al [12] investigated on a new shape sensor, ShapeTape^{TM} from Measurand Inc. ShapeTape^{TM} is an array of fiber optic curvature sensors laminated on a thin flexible ribbon substrate/tape, arranged to sense its bends and twist. This resulted a more effective vibration damping controller.

Apart from active control techniques, passive damping techniques are robust, effective and fail safe. The most important property of these techniques is that they don't require actuation energy to obtain the necessary damping of the flexible link. Passive constrained layer damping (PCLD) is an old technique to suppress vibrations. In combination with active control techniques, PCLD treatment can be made even more effective. This technique is called active constrained layer damping (ACLD) treatment. After thorough literature survey only one reference i.e. [13] was obtained showing the implementation of passive layer damping techniques to the flexible link manipulator. In this work, NASTRAN finite element analysis was used for the evaluation of the effectiveness of viscoelastic damping treatment as passive control for large flexible space manipulators.

Swallow [14] first introduced the concept of structural vibration reduction with constrained layer damping treatment. Kervin [15] presented the first analysis of the problem. Due to constraints of cost, full length VEM layer is not preferable. Partial treatments with certain length of VEM layers or multiple patches of small length are more beneficial. Nokes and Nelson [16] were among the earliest investigators to provide a theoretical and experimental study for partial treatment technique. A thorough analytical study was provided by Lall et al [17, 18] for beam and plate structures respectively. For enhancing the effectiveness of PCLD treatment, researchers like Whittier [19], proposed that the shear angle of the Viscoelastic layer could further be increased using a stand-of-layer (SOL) or spacer layer to the PCLD treatment between the vibrating structure and the constraining layer. This SOL layer moves the VEM layer and constraining layer farther from the neutral axis of the vibrating structure. This displacement which the SOL layer imposes magnifies the shear strain in the Viscoelastic layer and thus its energy dissipation. By choosing the specific material of the SOL layer, the overall damping of the treatment may be increased. Falugi [20, 21], Parin et al [22], Garrison and Miles [23] and Yellin et al

[24] presented an analytical model for the random response of a flexible structures partially treated with SOL layer.

Present paper investigates the vibration behavior and control of axial deformation and chord wise bending of a flexible link with partially covered PCLD treatment. As an extension of this work, the PCLD treatment with **SOL layer was** studied. Since the beam taken is rotating in horizontal plane, gravitational effect and rotary inertia are neglected. The stress strain relationship for the VEM layer is described by complex modulus. Hamilton principle in conjunction with Finite Element Method (FEM) is used to derive the equations of motion. Proportional-Integral-Derivative (PID) controller is designed for hub based angle-sensor and torque motor as actuator. The effects of thickness of SOL layer and shear modulus of SOL layer are studied. The effect of each parameter on the damping ratios and damped natural frequencies is investigated. PID controller designed using Pattern Search technique is used as primary feedback to regulate the hub motion. LQG controller was used as secondary feedback to control the hub by taking feedback from the PVDF sensor attached on the flexible arm. The effect of displacement feedback from PVDF sensor to PZT actuator (attached to the flexible arm) is also studied.

2. System Description and Finite Element Modeling

2.1 Basic Relationships

Flexible link attached to the hub is rotating as shown in the figure (1). The length of the flexible link is L.

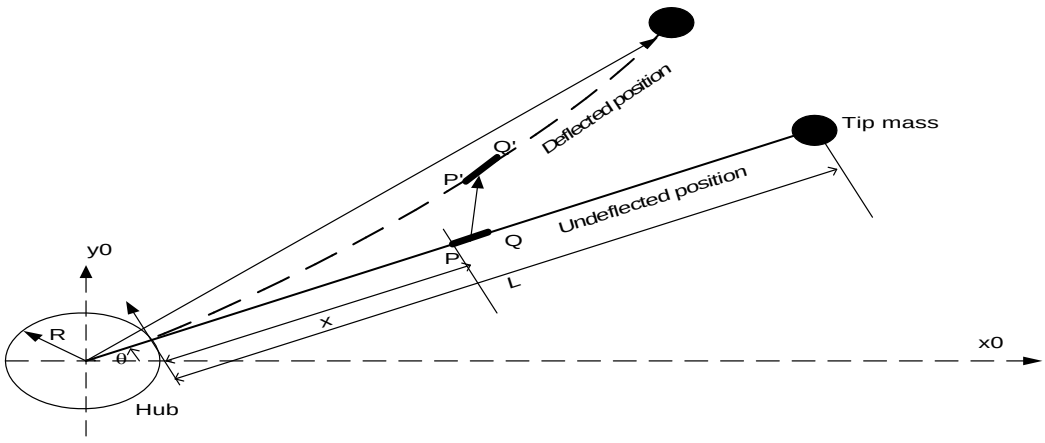

Figure 1 Schematic of flexible link

Figure (2) shows the flexible manipulator with different layer damping (LD) techniques. Figure (3) shows the cross-section and field variables of the beam with respective LD treatments.

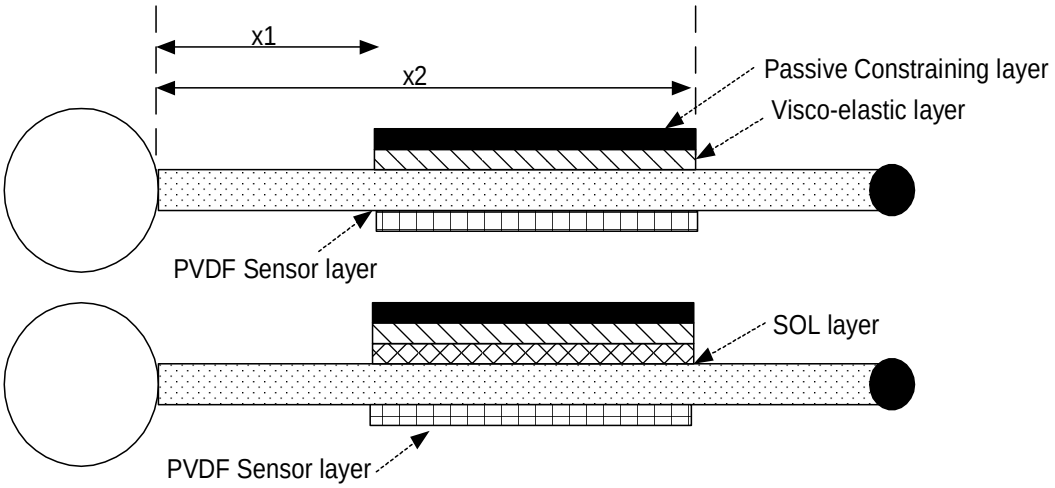

Figure 2:-Flexible link manipulator link with different layer damping techniques

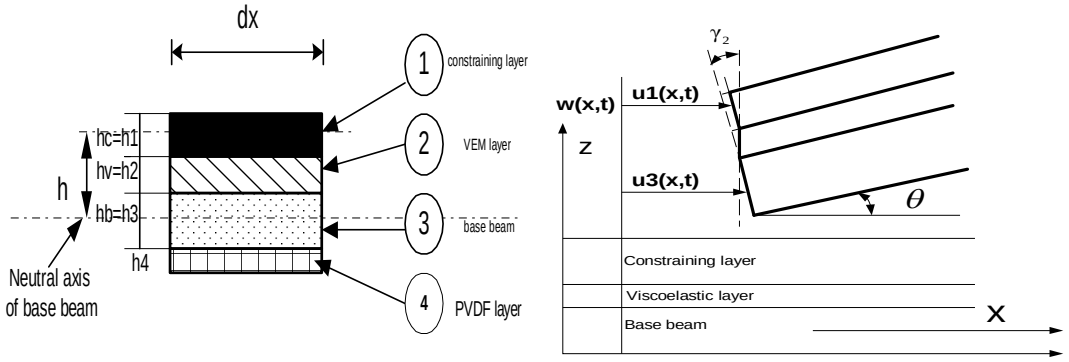

(a) PCLD (cross section) (b) PCLD (field variables)

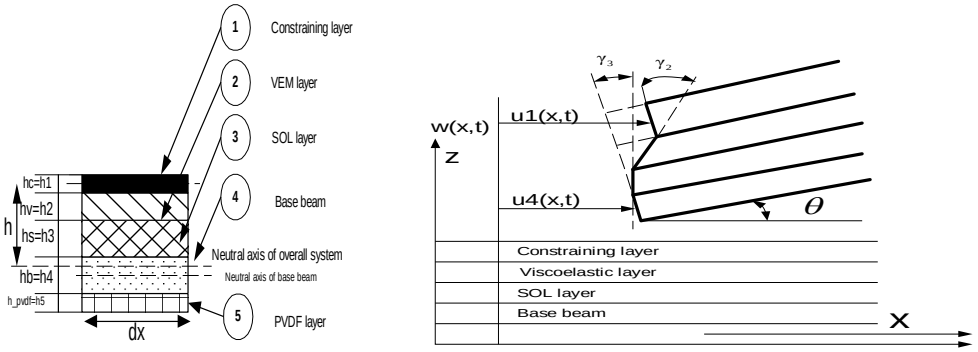

(c) PCLD with SOL layer (cross section) (d) PCLD with SOL layer (field variable)

Figure 3 Cross-section field variables of flexible link with different layer damping treatments

The base beam and constraining layer can be modeled as Euler-Bernoulli beams. For the continuity of displacements at the interface between the layers the relation between shear angle (strain) and various displacements is as per reference [24].

- **PCLD Treatment**

The upper surface of host structure or the base beam is attached with a Viscoelastic Material (VEM) layer. The VEM layer in turn is constrained by a passive constraining layer. For simplicity, the constrained layer is numbered as 1, VEM layer as no. 2, the base beam as no. 3 and sensor layer (i.e. PVDF on the opposite side of the base beam) as no. 4. The base beam and constraining layer can be modeled as Euler-Bernoulli beam. For continuity of displacements at the interface between the layers the relation between shear angle and various displacements is as under:

$$\varepsilon_1 = \frac{\partial u_1}{\partial x} = \frac{\partial u_{1m}}{\partial x} - z_1 \frac{\partial^2 w}{\partial x^2} \quad (1a)$$

$$\varepsilon_2 = \frac{\partial u_2}{\partial x} = \frac{\partial u_{2m}}{\partial x} - z_2 \frac{\partial^2 w}{\partial x^2} \quad (1b)$$

$$\varepsilon_3 = \frac{\partial u_3}{\partial x} = \frac{\partial u_{3m}}{\partial x} - z_3 \frac{\partial^2 w}{\partial x^2} \quad (1c)$$

$$\varepsilon_4 = \frac{\partial u_4}{\partial x} = \frac{\partial u_{4m}}{\partial x} - z_4 \frac{\partial^2 w}{\partial x^2} \quad (1d)$$

$$\gamma_2 = \frac{u_{1m} - u_{3m}}{h_2} + \frac{h}{h_2}\theta \quad (1e)$$

where

$$h = h_2 + \frac{(h_1 + h_3)}{2} \quad (1f)$$

and θ denotes the slope. u and w denote the longitudinal and transverse displacements respectively. h_1 , h_2 , h_3 and h_4 denote the thickness of constraining layer, VEM layer, base beam and sensor layer respectively. The shear stress developed in VEM layers is denoted by τ_2. The shear strain of the VEM layer is represented by γ_2. u_1, u_2, u_3 and u_4 are the longitudinal displacement of the constraining layer, VEM layer, the base beam and sensor layer respectively and w is the transverse displacement of all the layers. The shear stress in VEM layers is given as

$$\tau_2 = G_2 \gamma_2 \quad (2)$$

- **PCLD Treatment with SOL layer**

One side of host structure or the base beam is attached with a VEM layer and SOL layer. The VEM layer in turn is constrained by a passive constraining layer. The Poly Vinylene Di Fluroride (PVDF) layer acts as sensor and is attached on the other side of the base beam. For simplicity, the constrained layer is numbered as 1, VEM layer as no. 2, SOL layer as no. 3, the base beam as no. 4 and sensor layer (i.e. PVDF layer) as no. 5. For continuity of displacements at the interface between the layers the relation

between shear angle and various displacements is as under:

$$u_2=\frac{(u_4+u_1)}{2}+\frac{(h_1-2h_3-h_4)}{4}\theta \quad (3a)$$

$$u_3=u_4-\frac{(h_1+h_4)}{2}\theta \quad (3b)$$

$$\gamma_3=\left[\frac{u_1-u_4}{h_3}+\frac{1}{2}\left(1+\frac{h_1+2h_2+2y_b}{2h_3}\right)\theta\right]-\left(\frac{h_2}{h_3}\right)\gamma_2$$

$$=\left[\frac{u_1-u_4}{h_3}+\frac{1}{2}\frac{h}{h_3}\theta\right]-\left(\frac{h_2}{h_3}\right)\gamma_2 \quad (3c)$$

where

$$h=y_b+h_2+h_3+h_1/2 \quad (3d)$$

and θ denotes the slope. u and w denote the longitudinal and transverse displacements respectively. h_1, h_4, h_2 and h_3 denote the thickness of constraining layer, base beam, Viscoelastic layer and Stand off layer respectively. The distance between the top surface of the base beam and the neutral axis of the overall system is denoted by y_b. The shear stress developed in VEM layer is denoted by τ_2. The shear strain of the VEM layer is represented by γ_2. Similarly shear stress developed in SOL layer is denoted by τ_3. The shear strain of the SOL layer is represented by γ_3. u_1 and u_4 are the longitudinal displacement of the constraining layer and the base beam respectively and w is the transverse displacement of the constraining layer as well as of the base beam. The shear stress in both the layers is given as:

$$\tau_3 = G_3\gamma_3 \quad \text{and} \quad \tau_2 = G_2\gamma_2 \quad (4a, b)$$

Since equal stress is developed in both the layers, hence

$$\tau_3 = \tau_2 \quad (5)$$

Relation (4 and 5) show that

$$\gamma_3 = \left(G_2/G_3\right)\gamma_2 \quad (6)$$

Solving equations (3) and (5-6), we get

$$\gamma_3=\left[\frac{u_1-u_4}{h_3}+\left(1+\frac{h_1+2h_2+2y_4}{2h_3}\right)\theta\right]\left(\frac{G_2}{G_3}\right)\Big/\left(\frac{h_2}{h_3}+\frac{G_2}{G_3}\right) \quad (7a)$$

$$\gamma_2=\left[\frac{u_1-u_4}{h_3}+\left(1+\frac{h_1+2h_2+2y_b}{2h_3}\right)\theta\right]\Big/\left(\frac{h_2}{h_3}+\frac{G_2}{G_3}\right) \quad (7b)$$

and θ denotes the slope.

2.2 The Shape functions:

Nodal displacements are given as

$$\{U\}_e=\left\{w_i\ \ \theta_i\ \ u_{b_i}\ \ u_{c_i}\ \ w_j\ \ \theta_j\ \ u_{b_j}\ \ u_{c_j}\right\}^T \quad (8)$$

The transverse displacement w, the rotation θ and the axial displacements of the

respective layers are expressed in the nodal displacements by finite element shape functions shown below

- **PCLD treatment**

The shape functions are given as:

$$w=\left[N_w\right]\{U\}_e,\quad \theta=\left[N_\theta\right]\{U\}_e,\quad u_1=\left[N_{u_1}\right]\{U\}_e,\ u_2=\left[N_{u_2}\right]\{U\}_e,$$
$$u_3=\left[N_{u_3}\right]\{U\}_e,\ u_4=\left[N_{u_4}\right]\{U\}_e \text{ and } \gamma_2=\left[N_{\gamma_2}\right]\{U\}_e \qquad (9\ a,b,c,d,e,f,g)$$

where the shape functions are per reference [17].

- **PCLD with SOL**

The shape functions for this treatment are given as :

$$w=\left[N_w\right]\{U\}_e,\quad \theta=\left[N_\theta\right]\{U\}_e,\quad u_1=\left[N_{u_1}\right]\{U\}_e,\ u_2=\left[N_{u_2}\right]\{U\}_e,$$
$$u_3=\left[N_{u_3}\right]\{U\}_e,\ u_4=\left[N_{u_4}\right]\{U\}_e,\ u_5=\left[N_{u_5}\right]\{U\}_e \qquad (10\ a,b,c,d,e,f,g)$$

and

$$\gamma_2=\left[N_{\gamma_2}\right]\{U\}_e \text{ and } \gamma_3=\left[N_{\gamma_3}\right]\{U\}_e \qquad (10\ h,\ i)$$

Using these shape functions, the newly constructed shape functions can be written as:

$$\left[N_{u_3}\right]=\left[N_{u_4}\right]-\left(\frac{h_4+h_3}{2}\right)\left[N_\theta\right]$$

$$\left[N_{u_2}\right]=\frac{1}{2}\left(\left[N_{u_1}\right]+\left[N_{u_4}\right]\right)+\left(\frac{h_1-2h_3-h_4}{4}\right)\left[N_\theta\right]$$

$$\left[N_{\gamma_3}\right]=\left[\frac{1}{h_s}\left(\left[N_{u_1}\right]-\left[N_{u_4}\right]\right)+\left(\frac{h_1+2h_3+2h_2+h_4}{2}\right)\left[N_\theta\right]\right]\left[\frac{G_2/G_3}{h_2/h_3+G_2/G_3}\right] \qquad (11\ a,\ b,\ c,\ d)$$

$$\left[N_{\gamma_2}\right]=\left[\frac{1}{h_s}\left(\left[N_{u_1}\right]-\left[N_{u_4}\right]\right)+\left(\frac{h_1+2h_3+2h_2+h_4}{2}\right)\left[N_\theta\right]\right]\left[\frac{G_2/G_3}{h_2/h_3+G_2/G_3}\right]$$

2.3 The Energies of the PCLD system:

For simplicity, all the energies are given for a single element. The total energy can be obtained by the combination of all the elements. Kinetic energy (T_e), strain energy (U_e) and as well as the work done (W_e) by external transverse load and external torque are discussed as below.

2.3.1 Kinetic energies -

The position vector p_k of a special point in the k^{th} layer at a distance x from the origin of the beam is given by:

$$\mathbf{p}_k = \begin{Bmatrix} (R+x+u_k)\cos(\theta) - w\sin(\theta) \\ (R+x+u_k)\sin(\theta) + w\cos(\theta) \end{Bmatrix} \tag{12}$$

$$\dot{\mathbf{p}}_k = \begin{bmatrix} -\{(R+x+u_k)\sin(\theta)+w\cos(\theta)\}\dot{\theta} + \dot{u}\cos(\theta) - \sin(\theta)\dot{w} \\ \{(R+x+u_k)\cos(\theta) - w\sin(\theta)\}\dot{\theta} - \dot{u}\sin(\theta) + \cos(\theta)\dot{w} \end{bmatrix} \tag{13}$$

where the dot denotes differentiation with respect to time t. R is the radius of the hub. The total kinetic energy of the complete system comprises the kinetic energies of constraining layer, base beam, SOL layer, sensor layer and VEM layer and is given as:

$$T_e = \frac{1}{2}\int_0^{L_e} b\sum_{k=1}^{5}\rho_k h_k(\dot{\mathbf{p}}_k^T\dot{\mathbf{p}}_k)\,dx \tag{14}$$

2.3.2 Potential energies -

The total potential energy of the complete system comprises the strain energies of constraining layer, base beam, VEM layer, SOL layer and Sensor layer (PVDF layer). For each individual part it is given as below

The potential energy of the constraining layer due to axial displacement is

$$U_{e_1} = \frac{1}{2}E_1 h_1 b\int_0^{L_e}\left(\frac{\partial u_1}{\partial x}\right)^2 dx \tag{15a}$$

In all type of treatments, this energy remains the same. The potential energy of the constraining layer due to transverse displacement is

$$U_{e_2} = \frac{1}{2}E_1 I_1\int_0^{L_e}\left(\frac{\partial^2 w}{\partial x^2}\right)^2 dx \tag{15b}$$

Similarly, for all type of treatments, the energy terms remains the same. The potential energy of the VEM layer due to axial displacement is

$$U_{e_3} = \frac{1}{2}E_2 h_2 b\int_0^{L_e}\left(\frac{\partial u_2}{\partial x}\right)^2 dx \tag{15c}$$

The potential energy of the VEM layer due to transverse displacement is

$$U_{e_4} = \frac{1}{2}E_2 I_2\int_0^{L_e}\left(\frac{\partial^2 w}{\partial x^2}\right)^2 dx \tag{15d}$$

The potential energy of the VEM layer due to shearing

$$U_{e_5} = \frac{1}{2}G_2 h_2 b\int_0^{L_e}\gamma_2^2\,dx \tag{15e}$$

The potential energy of the SOL layer due to axial displacement is

$$U_{e_6} = \frac{1}{2}E_3 h_3 b\int_0^{L_e}\left(\frac{\partial u_3}{\partial x}\right)^2 dx \tag{15f}$$

The potential energy of the SOL layer due to transverse displacement is

$$\boldsymbol{U}_{e_7} = \frac{1}{2} E_3 I_3 \int_0^{L_e} \left(\frac{\partial^2 w}{\partial x^2} \right)^2 dx \quad (15g)$$

The potential energy of the SOL layer due to shearing is

$$U_{e_8} = \frac{1}{2} G_3 \, h_3 b \int_0^{L_e} \gamma_3^2 \, dx \quad (15h)$$

The potential energy of the base beam due to axial displacement is

$$\boldsymbol{U}_{e_9} = \frac{1}{2} E_4 h_4 b \int_0^{L_e} \left(\frac{\partial u_4}{\partial x} \right)^2 dx \quad (15i)$$

For PCLD treatment without SOL layer the potential energy of the base beam due to axial displacement is

$$\boldsymbol{U}_{e_9} = \frac{1}{2} E_3 h_3 b \int_0^{L_e} \left(\frac{\partial u_3}{\partial x} \right)^2 dx \quad (15j)$$

The potential energy of the base beam due to transverse displacement for PCLD treatment

$$\boldsymbol{U}_{e10} = \frac{1}{2} E_3 I_3 \int_0^{L_e} \left(\frac{\partial^2 w}{\partial x^2} \right)^2 dx \quad (15k)$$

However, for the PCLD treatment with SOL layer is

$$\boldsymbol{U}_{e10} = \frac{1}{2} E_4 I_4 \int_0^{L_e} \left(\frac{\partial^2 w}{\partial x^2} \right)^2 dx \quad (15l)$$

The potential energy of the sensor layer due to axial displacement for PCLD is

$$\boldsymbol{U}_{e_{11}} = \frac{1}{2} E_4 h_4 b \int_0^{L_e} \left(\frac{\partial u_4}{\partial x} \right)^2 dx \quad (15m)$$

However for the PCLD treatment with SOL layer it is

$$\boldsymbol{U}_{e_{11}} = \frac{1}{2} E_5 h_5 b \int_0^{L_e} \left(\frac{\partial u_5}{\partial x} \right)^2 dx \quad (15n)$$

The potential energy of the sensor layer due to transverse displacement for PCLD treatment

$$\boldsymbol{U}_{12} = \frac{1}{2} E_4 I_4 \int_0^{L_e} \left(\frac{\partial^2 w}{\partial x^2} \right)^2 dx \quad (15o)$$

However, for the PCLD with SOL layer

$$\boldsymbol{U}_{12} = \frac{1}{2} E_5 I_5 \int_0^{L_e} \left(\frac{\partial^2 w}{\partial x^2} \right)^2 dx \quad (15p)$$

2.4 Work done

Forces exerted on the system are

a) The externally applied mechanical force.

b) The externally applied torque at the hub.
Neglecting the external forces, the work done W_2 by the applied hub torque τ is given by

$$W_e = \tau\theta \tag{16}$$

2.5 Equations of Motion

Using Hamilton's principle, the equations of motion for an ACLD element can be written as:

$$\int_{t_1}^{t_2} \delta\left(T - \sum_{j=1}^{13} U_j\right) dt + \int_{t_1}^{t_2} \delta\left(\sum_{j=1}^{3} W_j\right) dt = 0 \tag{17}$$

For a single element with PCLD treatment, defining the element coefficients and matrices as follows:

$$J_i = \text{M.O.I of the hub} + \int_0^{L_e} \sum_{k=1,2,3,4} \rho_k h_k b (R + x_i + x)^2 dx \tag{18a}$$

For PCLD treatment with SOL layer, the corresponding relation becomes

$$J_i = \text{M.O.I of the hub} + \int_0^{L_e} \sum_{k=1,2,3,4,5} \rho_k h_k b (R + x_i + x)^2 dx \tag{18b}$$

The elemental mass matrix for the PCLD treatment is given as

$$\left[\mathbf{M_i}\right] = \int_0^{L_e} \sum_{k=1}^{4} \rho_k h_k b \left(\mathbf{N}_k^T \mathbf{N}_k + \mathbf{N}_w^T \mathbf{N}_w\right) dx \tag{18c}$$

For PCLD treatment with SOL layer, the corresponding relation becomes

$$\left[\mathbf{M_i}\right] = \int_0^{L_e} \sum_{k=1}^{5} \rho_k h_k b \left(\mathbf{N}_k^T \mathbf{N}_k + \mathbf{N}_w^T \mathbf{N}_w\right) dx \tag{18d}$$

Similarly, the elemental stiffness matrix for the PCLD treatment is given as

$$\left[\mathbf{K}_i\right] = \int_0^{L_e} \sum_{k=1}^{4} \left[E_k h_k b \left\{ \left(\frac{\partial \mathbf{N}_k}{\partial x}\right)^T \left(\frac{\partial \mathbf{N}_k}{\partial x}\right) \right\} + E_k I_k \left\{ \left(\frac{\partial^2 \mathbf{N}_w}{\partial x^2}\right)^T \left(\frac{\partial^2 \mathbf{N}_w}{\partial x^2}\right) \right\} \right] dx \tag{18e}$$

For PCLD treatment with SOL layer, the corresponding relation becomes

$$\left[\mathbf{K}_i\right] = \int_0^{L_e} \sum_{k=1}^{5} \left[E_k h_k b \left\{ \left(\frac{\partial \mathbf{N}_k}{\partial x}\right)^T \left(\frac{\partial \mathbf{N}_k}{\partial x}\right) \right\} + E_k I_k \left\{ \left(\frac{\partial^2 \mathbf{N}_w}{\partial x^2}\right)^T \left(\frac{\partial^2 \mathbf{N}_w}{\partial x^2}\right) \right\} \right] dx \tag{18f}$$

The other parameters like $\left\{\mathbf{V}_{1_i}\right\}$, $\left\{\mathbf{V}_{2_i}\right\}$, $\left[\mathbf{V}_{3_i}\right]$ and $\left[\mathbf{V}_{4_i}\right]$ will be modified according to the type of treatment as shown below:

- **PCLD treatment**

$$\left\{\mathbf{V}_{1_i}\right\} = \int_0^{L_e} \sum_{k=1}^{4} \left[\rho_k h_k b (x_i + x)\right] \mathbf{N}_k dx + R \int_0^{L_e} \sum_{k=1}^{4} \left[\rho_k h_k b\right] \mathbf{N}_k dx \tag{18g}$$

$$\left\{\mathbf{V}_{2_i}\right\} = \int_0^{L_e} \left[\sum_{k=1}^{4} \rho_k h_k b (x_i + x) \right] \mathbf{N}_w dx + R \int_0^{L_e} \left[\sum_{k=1}^{4} \rho_k h_k b \right] \mathbf{N}_w dx \tag{18h}$$

$$\left[\mathbf{V}_{3_i}\right]=\frac{1}{2}\int_0^{L_e}\sum_{k=1}^{4}\rho_k h_k b\left[L^2-(x_i+x)^2\right]\left\{\left(\frac{\partial\,\mathbf{N}_w}{\partial x}\right)^T\left(\frac{\partial \mathbf{N}_w}{\partial x}\right)\right\}dx \tag{18i}$$

$$\left[\mathbf{V}_{4_i}\right]=G_2 h_2 b\int_0^{L_e}\left[\mathbf{N}_{\gamma 2}\right]^T\left[\mathbf{N}_{\gamma 2}\right]dx \tag{18j}$$

- **PCLD treatment with SOL layer**

$$\left\{\mathbf{V}_{1_i}\right\}=\int_0^{L_e}\sum_{k=1}^{5}\left[\rho_k h_k b(x_i+x)\right]\mathbf{N}_k dx+R\int_0^{L_e}\sum_{k=1}^{5}\left[\rho_k h_k b\right]\mathbf{N}_k dx \tag{18k}$$

$$\left\{\mathbf{V}_{2_i}\right\}=\int_0^{L_e}\left[\sum_{k=1}^{5}\rho_k h_k b(x_i+x)\right]\mathbf{N}_w dx+R\int_0^{L_e}\left[\sum_{k=1}^{5}\rho_k h_k b\right]\mathbf{N}_w dx \tag{18l}$$

$$\left[\mathbf{V}_{3_i}\right]=\frac{1}{2}\int_0^{L_e}\sum_{k=1}^{5}\rho_k h_k b\left[L^2-(x_i+x)\right]\left\{\left(\frac{\partial\,\mathbf{N}_w}{\partial x}\right)^T\left(\frac{\partial \mathbf{N}_w}{\partial x}\right)\right\}dx \tag{18m}$$

$$\left[\mathbf{V}_{4_i}\right]=G_2 h_2 b\int_0^{L_e}\left[\mathbf{N}_{\gamma 2}\right]^T\left[\mathbf{N}_{\gamma 2}\right]dx+G_3 h_3 b\int_0^{L_e}\left[\mathbf{N}_{\gamma 3}\right]^T\left[\mathbf{N}_{\gamma 3}\right]dx \tag{18n}$$

In all the above equations 'x' is the distance from the clamped end to the left node of the element under consideration. J_i is the moment of inertia of the i^{th} element about the clamped end. $[\mathbf{M}_i]$ and $[\mathbf{K}_i]$ are the elemental mass and stiffness matrices respectively. $[\mathbf{V_{3i}}]$ and $[\mathbf{V_{4i}}]$ are due to centrifugal force and shear deformation respectively due to base beam, VEM layer, constraining layer and SOL layer. After using Hamilton's Principle, the equations of motion at the element level can be written as

$$\begin{bmatrix} M_{\theta\theta i} & \left\{\mathbf{M}_{\theta q i}\right\} \\ \left\{\mathbf{M}_{q\theta i}\right\} & \left[\mathbf{M}_{qqi}\right]\end{bmatrix}\begin{Bmatrix}\ddot{\theta} \\ \left\{\ddot{\mathbf{U}}\right\}_i\end{Bmatrix}+\begin{bmatrix}0 & \{0\} \\ \{0\} & \left[\mathbf{K}_{qqi}\right]\end{bmatrix}\begin{Bmatrix}\theta \\ \{\mathbf{U}\}_i\end{Bmatrix}=\begin{bmatrix}F_{\theta i} \\ \{0\}\end{bmatrix} \tag{19}$$

where

$$M_{\theta\theta i}=J_i+2\left\{V_{1i}\right\}\left\{q_i\right\} \tag{20a}$$

$$\left\{\mathbf{M}_{\theta q i}\right\}=\left\{\mathbf{M}_{q\theta i}\right\}^T=\left\{\mathbf{V}_{2i}\right\} \tag{20b}$$

$$\left[\mathbf{M}_{qqi}\right]=\left[\mathbf{M}_i\right] \tag{20c}$$

$$\left[\mathbf{K}_{qqi}\right]=\left[\mathbf{K}_i\right]+\left[\mathbf{V}_{4i}\right] \tag{20d}$$

$$F_{\theta i}=\tau \tag{20e}$$

in which $M_{\theta\theta i}$ is the rotational inertia of the system, $\left[\mathbf{M}_{qqi}\right]$ is the generalized mass matrix, $\left\{\mathbf{M}_{\theta qi}\right\}$ is the non-linear inertia coupling between rigid body and the elastic deformations, $\left[\mathbf{K}_{qqi}\right]$ is the generalized stiffness matrix. The above equation without subscript i denotes the global form of corresponding elemental co-efficient matrices.

2.6 Contribution of tip mass in system dynamics

The tip load M_p attached at the free end of the will contribute to the additional

moment of inertia. The term $\frac{1}{2}M_p(R+L)^2$ will be added in equation (20a). Also, this mass will contribute to the dynamics of the system through its kinetic energy. Only the translational kinetic energy of the tip mass will be taken into account because the rotational inertia can be neglected. Similarly, the effect on other parameters can be obtained. The reader is directed to [9] for greater details.

3. Implementation to Flexible Arm

A flexible arm of length 950 mm and dimensions as shown in table (1) is taken for investigation. Figure (4) shows the frequency response function (FRF) from torque applied at the hub to the hub angle. With the application of the PCLD treatment amplitude reduction for the first mode is 9 dB. However, with using SOL layer in the PCLD treatment the amplitude reduction is 29 dB as compared to the case where no PCLD treatment was applied. The contribution of the PCLD treatment is approximately nil for the second mode of vibration for the present location of the treatment. However, with the application of SOL in the PCLD treatment, 27 dB amplitude reductions are possible for the second mode. Figure (5) shows the FRF from the torque applied at the hub to the tip displacement. With PCLD treatment 9 dB amplitude reduction is possible for the first mode as compared to plain flexible arm with no treatment. The amplitude reduction for the second mode is 4 dB with PCLD treatment. However, with the application of SOL in the PCLD treatment, the corresponding values are 27.5 dB and 15 dB respectively.

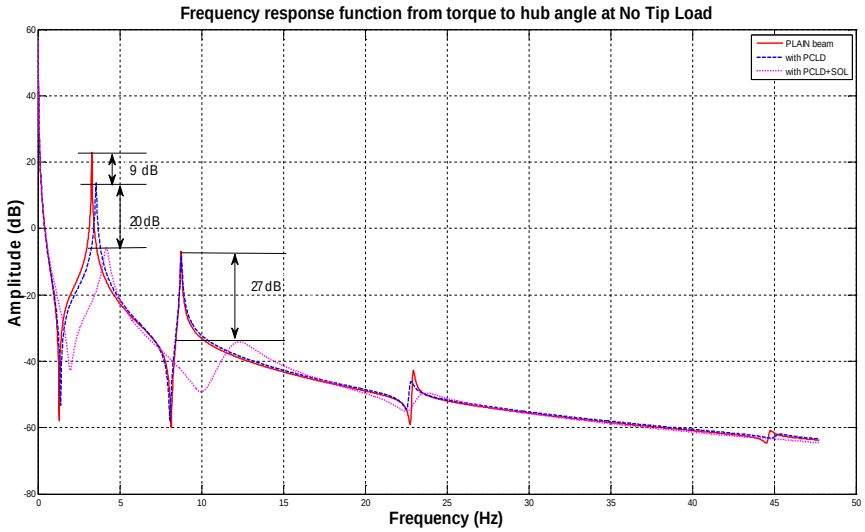

Figure 4:- Frequency response function of the manipulator torque to hub angle at No tip Load

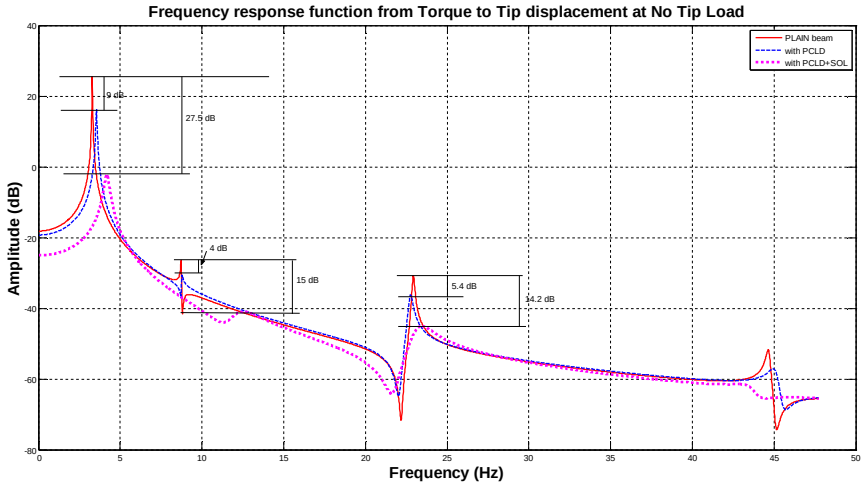

Figure 5. Frequency response function of the manipulator from torque to Tip displacement at No tip Load

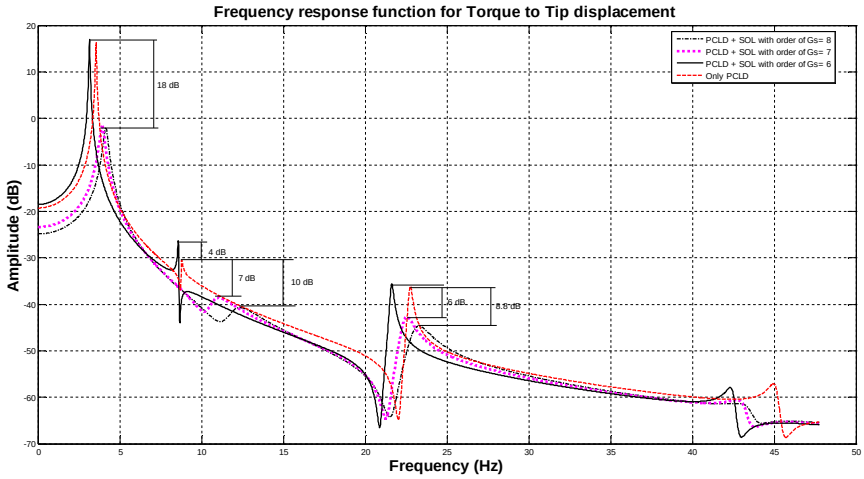

Figure 6. Frequency response function of the manipulator from torque to tip displacement at No tip Load at various values of shear modulus

4. Experimentation

4.1 Details of experimental Setup

To check the authenticity of the theoretical results experimental setup was generated. Figure (7) shows the schematic of the flexible link with layer damping technique. Length of the link is 950 mm. A passive constraining layer of aluminum of 0.1 mm is applied. Length of the treated portion is 200 mm and the treatment is done at a distance of 100 mm from the hub. DYAD 606 and ISD 112 are the professional material names for SOL and VEM layer respectively. For ACLD treatment, a PZT patch of 0.2 mm thickness was attached on the VEM layer and a PVDF layer of 0.1 mm was attached on the other side of the base beam. The thickness of the VEM layer is 1.0 mm and SOL layer is 2.286 mm. The base beam is made of steel and is of the thickness 1.4mm. The length of the PZT patch is 200 mm. Width of the PZT patch is

same as that of the base beam i.e. 36 mm. Other dimensions can be found in table (1). An analog low pass filter with cut-off frequency equal to just above the fourth resonance frequency of the vibrating structure (i.e. 45 Hz in the present case) was applied to remove the influence of higher modes. To remove the DC offset a high pass filter was used. The spectrum analyzer HP35670A from HP technologies was used to create signals of various types for system identification purpose. The other important material and electrical properties of the different materials are shown in table (1 and 2). Practically the shear modulus of DYAD 606 (SOL layer material) is 100-300 times that of ISD 112 (VEM layer). Small variation in results can be attributed to the reasons that the strain developed in the base beam varies due to loose adhesive bond of the gluing adhesives and the variation in the properties of the PZT, aluminium, VEM, SOL layer material parameters and compressional damping factor which needs addition of separate transverse displacement for the constraining layer. The controller was implemented using a dSPACE DS1103 rapid prototyping Controller board together with MATLAB and SIMULINK environment. The sampling frequency was set as 30 kHz. A dc brush servo motor GM4040-41 was used. The motor was driven by a Glentek GA377 pulse width modulation servo amplifier. The motor has a continuous stall torque of 3.54 Nm and a maximum bandwidth of 58 Hz. The shaft encoder of the motor was used to measure the hub angle of rotation with resolution 0.072^{o}.

Table 1- Geometrical and material properties of the structure (flexible arm)

Member	Thickness (mm)	Density (Kg/m3)	Young's Modulus (N/m2)	Shear Modulus (N/m2)
Flexible manipulator	1.4	7800	210×10^{9}	-
Viscoelastic layer	1	1390	-	0.2615×10^{6} (1+0.38i)
Constraining layer PZT (actuator) layer	0.2	7600	49×10^{9}	-
PVDF (sensor) layer	0.1	1240	-	-
SOL layer	2.286	1000	0.5230×10^{9} (1+0.38i)	0.2615×10^{9} (1+0.38i)

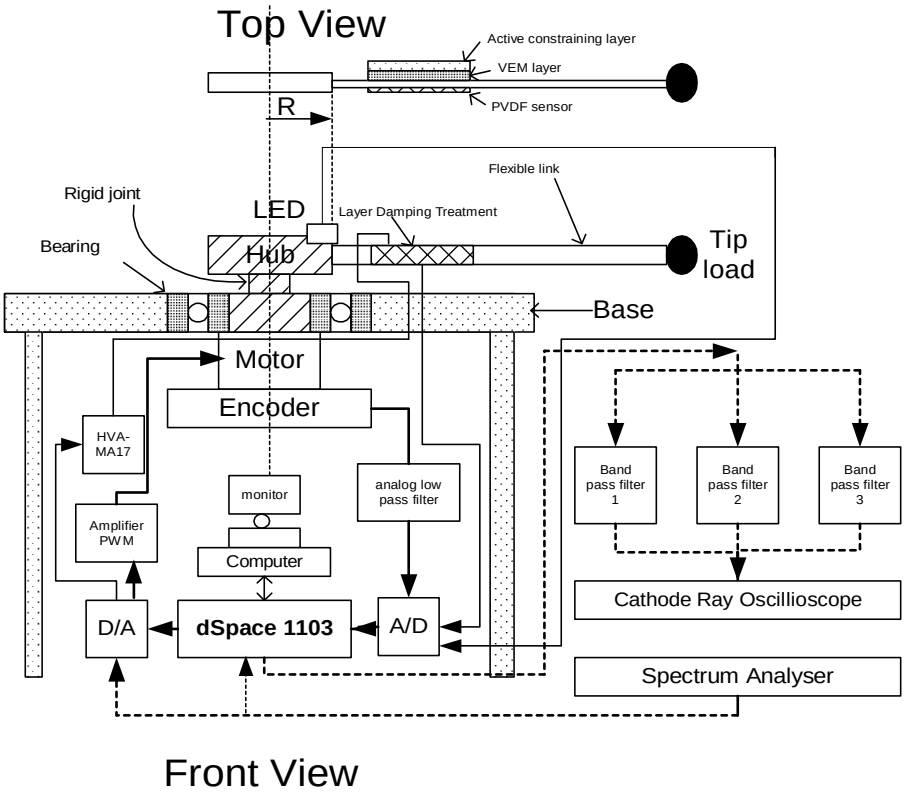

Figure. (7) Schematic of Experimental setup

Table 2:- Electrical Properties of PZT

Property	**Symbol**	**Value**
Piezoelectric charge constant (m V^{-1})	d_{31}	$171x10^{-12}$
Electromechanical Coupling factor	k_{31}	0.12
Piezoelectric voltage constant (VmN^{-1})	g_{31}	$216x10^{-3}$
Dielectric constant	k_{3t}	12

Table 3:- Comparison of Theoretical and Experimental results

	Natural Frequencies		**Damping Ratio's**	
	mode1	**mode2**	**mode1**	**mode2**
Theoretical	1.57	9.10	0.0452	0.0584
Experimental	1.65	9.5	0.0410	0.0522

4.2 Experimental non-parametric system identification

For an accurate identification, any arbitrary signal may not be suitable. The input data supplied to the system for system identification should be informative [27]. Both for open loop (OL) and CL operations, 'informative' means that the input should be persistently exciting of a certain order; i.e. it contains sufficiently many distinct

frequencies [27]. In the present case, to excite the system in OL conditions, the multisine wave with minimum crest factor [19] and moderate magnitude of the excitation is used. The duration of the excitation signal was chosen to be 10 second**.** The frequency content of the signal was 0-50 Hz. To minimize the measurement noise the experiment was repeated several times. The frequency response function (FRF) was obtained from time domain data using Welch's algorithm [28]. 100 spectral lines were used for constructing the FRF of the flexible link. Table (3) represents the comparison between theoretical and experimental vibration parameters. Figure (8) shows the comparison of theoretical and experimental frequency response function.

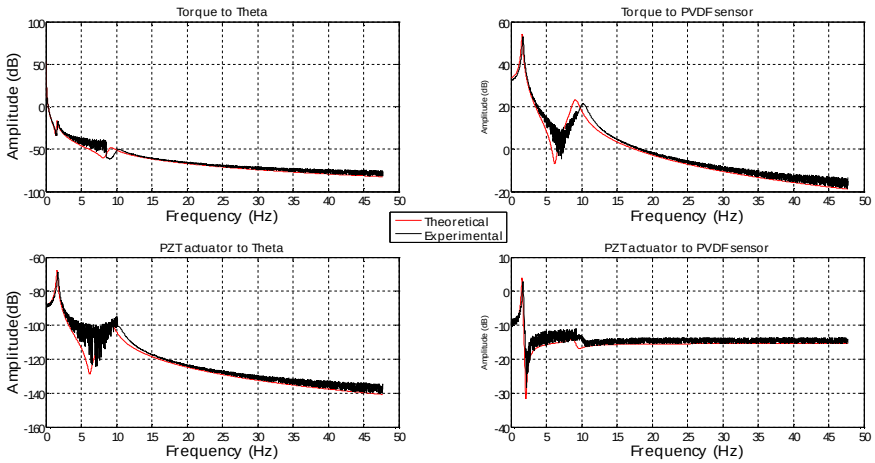

Figure 8 Comparison of theoretical and experimental frequency response function

5. Grey Box Sub-Space Parametric System Identification

After the calculations of FRF obtained using Welch's algorithm, the next step is to find the parameters of the system. The single link flexible manipulator can be seen as the following transfer functions connected in parallel

$$\frac{1}{I_T s^2}, \frac{\phi_1^1}{s^2 + 2\xi_1\omega_1 s + \omega_1^2}, \ldots\ldots, \frac{\phi_1^N}{s^2 + 2\xi_N\omega_N s + \omega_N^2} \tag{21}$$

where N is the total number of modes considered. ξ_N is the damping ratio of the Nth mode, ω_N is the Nth frequency of the flexible manipulator. I_T is the mass moment of inertia of the manipulator. The total system can be represented as transfer function in polynomial form with ratio of two polynomials. Lower polynomial represents the poles of the system and upper polynomial represents the zeros of the system. Using identification techniques the poles can be identified and hence the natural frequencies and the damping ratios.

The second step is to find ϕs. These are the product of mode shapes at the sensor and actuator location. Assuming ϕ_1^1 …. ϕ_1^N as unity the FRF of the sub-systems is calculated and represented as T_0, T_1,…..T_N. Let the real part and imaginary part of this can be represented as T^R and T^I, the following equation holds [29]

$$\begin{bmatrix} T_0^R(\omega_1) & T_1^R(\omega_1) & T_2^R(\omega_1) & \cdots & T_N^R(\omega_1) \\ T_0^R(\omega_2) & T_1^R(\omega_2) & T_2^R(\omega_2) & \cdots & T_N^R(\omega_2) \\ \vdots & \vdots & \vdots & \vdots & \vdots \\ T_0^R(\omega_M) & T_1^R(\omega_M) & T_2^R(\omega_M) & \cdots & T_N^R(\omega_M) \\ T_0^I(\omega_1) & T_1^I(\omega_1) & T_2^I(\omega_1) & \cdots & T_N^I(\omega_1) \\ T_0^I(\omega_2) & T_1^I(\omega_2) & T_2^I(\omega_2) & \cdots & T_N^I(\omega_2) \\ \vdots & \vdots & \vdots & \vdots & \vdots \\ T_0^I(\omega_M) & T_1^I(\omega_M) & T_2^I(\omega_M) & \cdots & T_N^I(\omega_M) \end{bmatrix} \begin{bmatrix} 1 \\ \phi_1^1 \\ \phi_1^2 \\ \vdots \\ \phi_1^N \end{bmatrix} = \begin{bmatrix} T^R(\omega_1) \\ T^R(\omega_2) \\ \vdots \\ T^R(\omega_N) \\ T^I(\omega_1) \\ T^I(\omega_2) \\ \vdots \\ T^I(\omega_N) \end{bmatrix} \tag{22}$$

where T^R and T^I represents the value of real and imaginary part of the overall transfer function at a particular frequency ω. Each term has its physical meaning in this type of system identification methodology. The state-space model obtained is given as:

$$A = \begin{bmatrix} 0 & 1 & 0 & 0 & \cdots & \cdots & 0 & 0 \\ 0 & 0 & 0 & 0 & \cdots & \cdots & 0 & 0 \\ 0 & 0 & 0 & 1 & \cdots & \cdots & 0 & 0 \\ 0 & 0 & -\omega_1^2 & -2\xi_1\omega_1 & \cdots & \cdots & 0 & 0 \\ \vdots & \vdots & \vdots & \vdots & \ddots & \ddots & \vdots & \vdots \\ \vdots & \vdots & \vdots & \vdots & \ddots & \ddots & \vdots & \vdots \\ 0 & 0 & 0 & 0 & \cdots & \cdots & 0 & 1 \\ 0 & 0 & 0 & 0 & \cdots & \cdots & -\omega_N^2 & -2\xi_N\omega_N \end{bmatrix} \tag{23}$$

$$B = \begin{bmatrix} 0 & 1/I_T & 0 & 1 & \cdots & \cdots & 0 & 1 \end{bmatrix}^T$$

$$C = \begin{bmatrix} 1 & 0 & \phi_1^1 & 0 & \cdots & \cdots & \phi_1^N & 0 \\ 0 & 0 & \phi_2^1 & 0 & \cdots & \cdots & \phi_2^N & 0 \end{bmatrix}$$

6 PID Control Design for Hub Regulation based on Pattern Search Method

6.1 PID Controller Design using Pattern Search Technique

Figure (9) shows the comparison of the actual response of the hub angle under the application of the PID controller. The same PID controller is applied to the manipulator without and with PCLD treatment with SOL layer. The maximum voltage developed in the PVDF sensor is -18 volt for a plain flexible manipulator. With the application of PCLD treatment with SOL layer the maximum voltage generated is -4 volt (Figure 10). Similar is the case with voltage on the positive side. Afterwards, LQG controller is applied to the manipulator with PCLD.

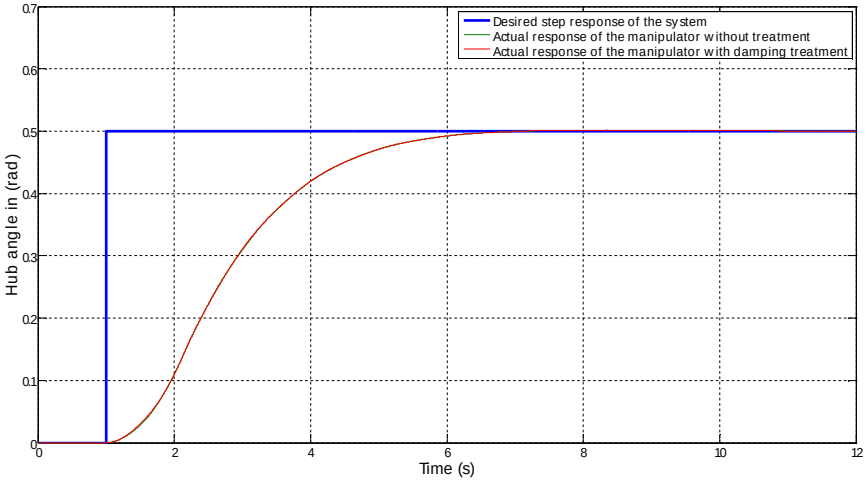

Figure 9 Comparison of rotational response of the system with and without damping treatment

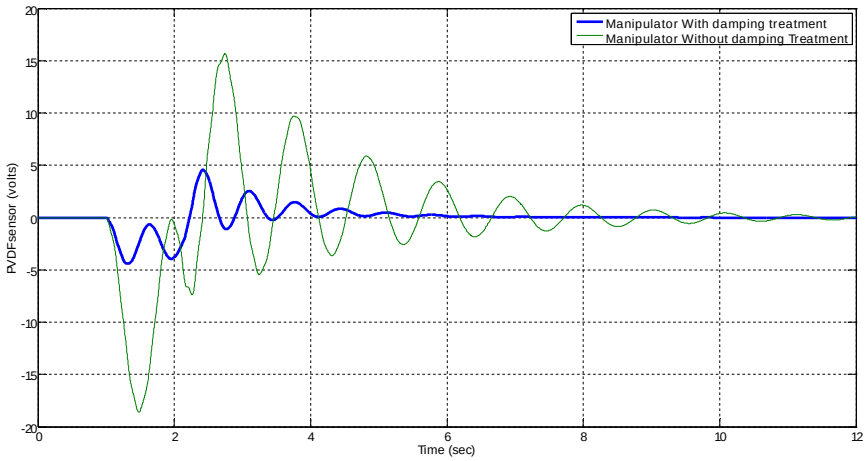

Figure 10 Comparison of response of the system at PVDF sensor with and without damping treatment

7. Linear Quadratic Gaussian Control and Kalman Filter Design

For a linear system given by equation (20) if all the states of the system are controllable, the system is said to be completely controllable. Observability means that the states of a system can be determined from a finite number of its most recent inputs and outputs. So the system matrices are checked for this test for Observability before designing the observer.

Due to various uncertainties the system dynamics is not constant. In such situations, LQR is found to be an excellent robust control system design methodology [31]. Let the system to be controlled be written in state space form as

$$\begin{aligned} \dot{\mathbf{X}}(t) &= \mathbf{A}\,\mathbf{X}(t) + \mathbf{B}\,\mathbf{u}(t) + \boldsymbol{\Gamma}\mathbf{w} \\ \mathbf{y}(t) &= \mathbf{C}\,\mathbf{X}(t) + \mathbf{v} \end{aligned} \tag{24}$$

where **w** and **v** are the 'white noises', namely zero – mean Gaussian stochastic processes which are uncorrelated in time, having covariances

$$E\left\{\boldsymbol{w}\boldsymbol{w}^T\right\} = \boldsymbol{W} \geq 0, \quad E\left\{\boldsymbol{v}\boldsymbol{v}^T\right\} = \boldsymbol{V} > 0 \tag{25a}$$

It is assumed that w and v are uncorrelated with each other namely

$$E\left\{\boldsymbol{w}\boldsymbol{v}^T\right\} = \boldsymbol{0} \tag{25b}$$

In optimal control problem it is to find the input **u** (t), to the plant such that a scalar quadratic cost function

$$J_1 = \lim_{T\to\infty} \mathrm{E}\left\{\int_0^{\mathrm{T}} \left(\mathbf{z}^{\mathrm{T}}\mathbf{Q}\mathbf{z} + \mathbf{u}^{\mathrm{T}}\mathbf{R}\mathbf{u}\right) dt\right\} \tag{26}$$

Using the gain matrix **K,** control inputs are calculated by the following equation

$$\mathbf{u}\,(\mathrm{t}) = -\,\mathbf{K}\,\mathbf{X}\,(\mathrm{t}) \tag{27}$$

7.1 Measurement of Noise Characteristics

It is important to estimate the noise characteristics of the measurement system so that accurate behavior of the overall system can be predicted. The noise characteristics of the measurement system consist of measurement noise and process noise. Since the measurement covariance matrix **V** and process covariance matrix **W** are required in Kalman filter calculations, these must be known before designing the Kalman Filter. These matrices depend upon measurement noise and process noise. Therefore, a mathematical model of the noise sequences is necessary. The measurement noise and process noise are assumed to be zero mean.

7.2 Kalman Filter design

Normally input – output data is available from experimental setup. To estimate the states of the system some form of estimator is required. In the present work Kalman filter is used as estimator. The Kalman – filter gain matrix **L** is given by [31]

$$\mathbf{L}=\mathbf{P_f}\,\mathbf{C}^{\mathbf{T}}\,\mathbf{V}^{-\mathbf{1}} \tag{28}$$

where $\mathbf{P_f}$ satisfies another algebraic equation

$$\mathbf{P_f}\mathbf{A}^{\mathbf{T}} + \mathbf{A}\mathbf{P_f} - \mathbf{P_f}\mathbf{C}^{\mathbf{T}}\mathbf{V}^{-\mathbf{1}}\mathbf{C}\mathbf{P_f} + \boldsymbol{\Gamma}\mathbf{W}\boldsymbol{\Gamma}^{\mathbf{T}} = \mathbf{0} \tag{29}$$

and $\mathbf{P_f} = \mathbf{P_f^T} \geq 0$

The matrices **K** and **L** exist, and the closed loop system is internally stable, provided the system with state space realizations (**A, B,** $\mathbf{Q}^{\mathbf{1/2}}$ **M**) and $(\mathbf{A}, \boldsymbol{\Gamma}\,\mathbf{W}^{\mathbf{1/2}}, \mathbf{C})$ are stablizable and detectable.

8. Results and Conclusion

Figure (11), shows the schematic of the controller design. The hub angle and the strain feedback from the PZT sensor is used to regulate the hub. The displacement feedback control is used in ACLD treatment. It is a collocated type of structure. Figure (12) shows the effect of feedback gain -2.

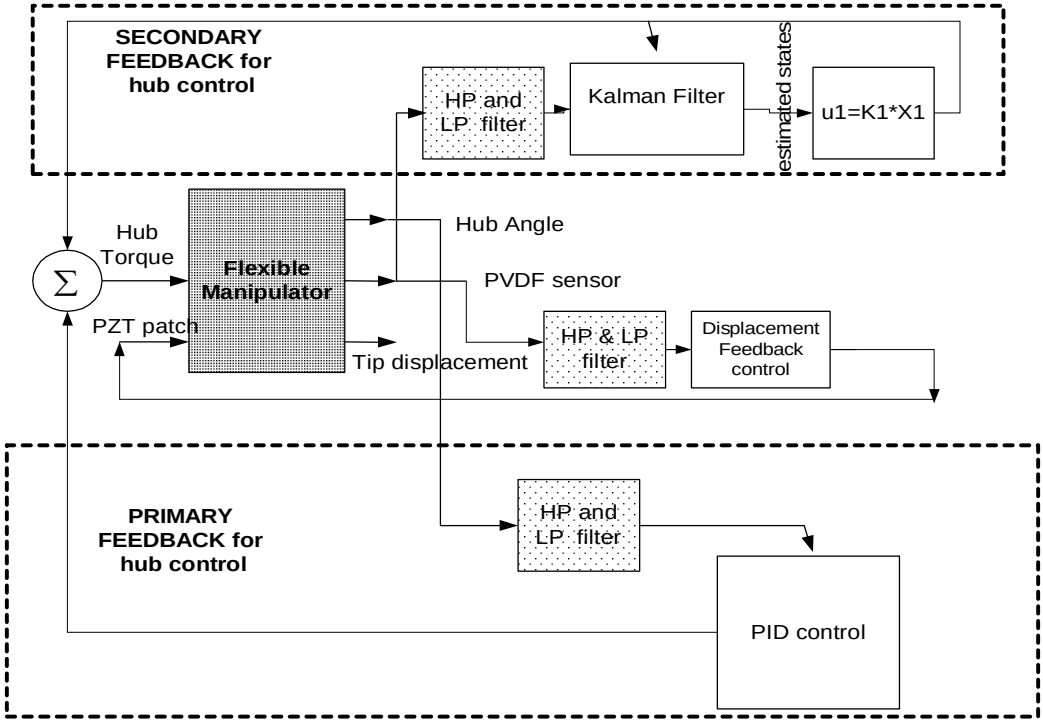

Figure 11: - Schematic of the LQG control applied

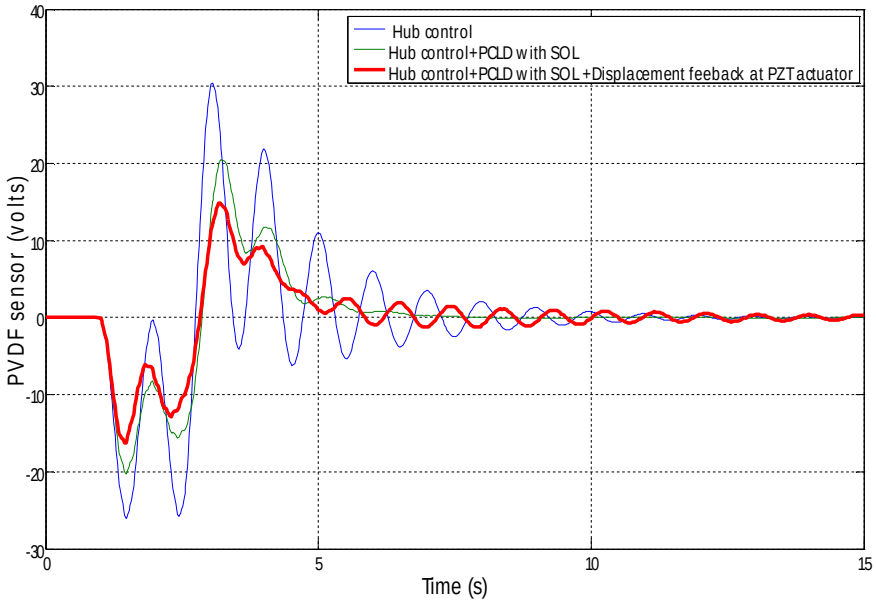

Figure 12:- Response of the system at displacement feedback control (gain=-1)

In the present work, PCLD and ACLD treatment is investigated to increase the damping efficiency of the flexible link manipulator. It has been observed that using

PCLD treatment, the percentage overshoot from the equilibrium position as well as duration of end – effector vibrations can be reduced. By using the SOL layer, the damping efficiency can be further increased. By making the constraining layer active, the percentage overshoot from the equilibrium position as well as duration of end – effector vibrations can be further reduced.

REFERENCES

1. Book, W.J, 1993, Controlled motion in an elastic world, ASME Journal of Dynamic Systems, Measurement and Control, 115, pp 252-261.
2. Moudgal, V.G., Passino, K.M., and Yurkovich, S, 1994, Rule-based control for a flexible link robot, IEEE Transactions on Control Systems Technology, 2, pp 392-405.
3. Choi, S.B., Cheong, C.C., and Shin, H.C, 1995, Sliding mode control of vibration in a single link flexible arm with parameter variations, Journal of Sound and Vibration, 179, pp. 737-748.
4. Choi, S.B., and Shin, H.C, 1996, A hybrid actuator scheme for robust position control of a flexible link manipulator, Journal of Robotic Systems, 13, pp 359-370.
5. Yang, H.J., Lian, F.L., and Fu, L.C, 1997, Nonlinear adaptive control for flexible link manipulators, IEEE Transactions on Robotics and Automation, 13, pp 140-8.
6. Canon, R.H, and Schmitz, E, 1984, Initial experiments on the end-point control of a flexible one-link robot, International Journal of Robotics Research, 3, pp 62-75.
7. Luo, Z.H, 1993, Direct strain feedback control of flexible robot arms: New theoretical and experimental results, Transactions on Automatic Control, 38, pp 1610-1622.
8. Sun, D., Mills, J.K., Shan, J., and Tso, S.K, 2004, A PZT actuator control of a single-link flexible manipulator based on linear velocity feedback and actuator placement, Journal of Mechatronics, 14, pp 381-401.
9. Shan, J., Liu, H.T, and Sun, D., 2005, Slewing and vibration control of a single-link flexible manipulator by positive position feedback (PPF), Journal of Mechatronics, 15, pp 487-503.
10. Sun, D., and Mills, J.K., 2002, Control of a rotating cantilever beam using a torque actuator and a distributed piezoelectric polymer actuator, Applied Acoustics, 63, pp 885-899.
11. Sun, D., Shan, J., Xu, Y., Liu, H.T., and Lam, C., 2005, Hybrid control of a rotational flexible beam using enhanced PD feedback with a nonlinear differentiator and PZT actuators, Smart Materials and Structure, 14, pp 69-78.
12. Gurses, K., Buckham, B.J. and Park, E.J., 2009, Vibration control of a single-link flexible manipulator using an array of fiber optic curvature sensors and PZT actuators, Journal of Mechatronics, 19, pp 167-77.
13. Alberts, T.E., Xia, H., and Chen, Y. 1992, Dynamic analysis to evaluate viscoelastic passive damping augmentation for the space shuttle remote manipulator system, ASME Journal of Dynamic Systems, Measurement and Control, 114, pp 468-75.
14. Swallow, W. 1939, An improved method of damping panel vibrations, British Patent Specification, 513.
15. Kervin, E.M., 1959, Damping of flexural waves by a constrained visco-elastic layer, Journal of Acoustical Society of America, 31, pp 952-962.
16. Nokes, D.S., and Nelson, F.C, 1968, Constrained layer damping with partial coverage, Shock and Vibration Bulletin, 38, pp 5-10.

17. Lall, A.K., Ansari, N.T., and Nackra, B.C, 1988, Damping analysis of partially covered sandwich beams, Journal of Sound and Vibration, 123(2), pp 247-259.
18. Lall, A.K., Ansari, N.T., and Nackra, B.C, 1987, Vibration and damping analysis of rectangular plate with partially covered constrained Viscoelastic layer, Transactions of ASME Journal of Vibration, Acoustics, Stress and Reliability in Design, 109, pp 241-247.
19. Whittier, J.S, 1959, The effect of configurational additions using Viscoelastic interfaces on the damping of a cantilever beam, Wright Air Development Center WADC Technical Report, pp 58-568.
20. Falugi, M., Moon, Y., and Arnold, R., 1989, Investigation of a four layer Viscoelastic constrained layer damping system, USAF/WL/FIBA/ASIAC: Report No. 189.1 A.
21. Falugi, M., 1991, Analysis of a five layer Viscoelastic constrained layer beam, Proceedings of Damping II, Paper No. CCB.
22. Parin, M., Rogers, L.C., Falugi, M., and Moon, Y., 1989, Practical Stand-off damping treatment for sheet metal, Proceedings of Damping II, Paper No. IBA.
23. Garrison, M.R., Miles, R.N., Sun, J.Q., and Bao, W, 1994, Random response of a plate partially covered by a constrained layer damper, Journal of Sound and Vibration, 172(2) pp. 231-245.
24. Yellin., M., Jessica, I.Y., Shen, G., Reinhall. Per, and Huang. Peter, Y.H., 2000, An Analytical and experimental analysis for a one-dimensional passive stand-off layer damping treatment, ASME Journal of Vibration and Acoustics,, 122, pp 440-447.
25. Mostafa, Abd-Elwahab., and Sherif. Hany, 2006, A Pre-tensioned layer damping as a new approach for vibration control of elastic beams, ASME Journal of Vibration and Acoustics, 128, pp. 338-346.
26. Kumar, S., Kumar, R., and Sehgal, R., 2011, Active vibration control of beams by combining pre-compressed layer damping and ACLD treatment: Theory and experimental implementation, ASME Journal of Vibration and Acoustics, 133, pp 61013(1-17)
27. Ljung L, 1999, System Identification- Theory for the user, Prentice Hall, New York.
28. Welch, P. D., 1967, The use of fast Fourier transform for the estimation of power spectra: A method based in time averaging over shot, modified periodograms, IEEE Transactions on Audio Electro acoustics, 15, pp 70-73.
29. Cavallo, A., Maria, G. D., Natale, C., and Pirozzi, S., 2007, Grey-Box identification of continuous-time models of flexible structures, IEEE Transactions on Control Systems Technology **, 15(**5), pp 967-981.
30. Torczon, V., 1997, On the convergence of pattern search algorithms, Siam Journal of Optimization, 7, pp 1–25.
31. Gu, D. W., Petkov, P. H., and Konstantinov, M. M., 2005, Robust control design with MATLAB, Springer-Verlag London.